The Journal of Neuroscience, January 1993, 13(1): 181–194

Multiple Modes of N-Type Calcium Channel Activity Distinguished by Differences in Gating Kinetics

Anne H. Delcour,[a] Diane Lipscombe,[b] and Richard W. Tsien

Department of Molecular and Cellular Physiology, Beckman Center, Stanford University Medical Center, Stanford, California 94305

In many neurons, N-type Ca^{2+} channels are a major Ca^{2+} entry pathway and strongly influence neurotransmitter release. We carried out cell-attached patch recordings (110 mM Ba^{2+} as charge carrier) to characterize the rapid opening and closing kinetics of N-type Ca^{2+} channel gating in frog sympathetic neurons. Single channels display at least three distinct patterns of gating, characterized as low-, medium-, and high-p_o modes on the basis of channel open probability (p_o) during depolarizing pulses to −10 mV. Spontaneous transitions from one mode to another are infrequent, with an exponential distribution of dwell times and mean sojourns of ~10 sec in each mode. Thus, a channel typically undergoes hundreds or thousands of open–closed transitions in one mode before switching to a different mode. Transitions between modes during a depolarization were occasionally detected, but were rare, as expected for infrequent modal switching. Within each mode, the activation kinetics were well described by a simple scheme (C2-C1-O), as previously reported for other types of Ca^{2+} channels. Rate constants are strikingly different from one mode to another, giving each mode its own characteristic kinetic signature. The gating behavior at −10 mV ranges from brief openings (~0.3 msec) and long closures (10–20 msec) for low-p_o gating to long openings (3 msec) and brief closures (~1 msec) for high-p_o gating. Intermediate values for mean open durations (~1.5 msec) and mean closed durations (~3 msec) were found for medium-p_o gating. In addition to being kinetically distinct, channel openings in the low-p_o mode often exhibit a unitary current ~0.2 pA larger than in the medium- or high-p_o mode. Each mode is characterized by its own voltage dependence: activation occurs at relatively negative potentials and is most steeply voltage dependent in the high-p_o mode, while activation requires very strong depolarizations and is weakly voltage dependent in the low-p_o mode. The proportion of time spent in the individual modes varies greatly from one patch to another, suggesting that modal gating may be subject to cellular control.

[Key words: ion channel, Ca^{2+} channel, gating modes, activation kinetics, sympathetic neurons, GTP-binding proteins]

N-type Ca^{2+} channels are a class of voltage-gated Ca^{2+} channels found almost exclusively in the nervous system. They are of interest for a number of reasons: they are the major pathway for Ca^{2+} entry in several different types of neuron (Tsien et al., 1988; Bean, 1989a; Hess, 1990), they can play a dominant role in controlling neurotransmitter release (Hirning et al., 1988; Stanley, 1991; Miller, 1992), and they are strongly modulated by neurotransmitters and other ligands (e.g., Tsien et al., 1988; Carbone and Swandulla, 1989; Beech et al., 1992).

Knowledge about N-type channels has grown steadily since their initial description in chick sensory neurons (Nowycky et al., 1985a; Aosaki and Kasai, 1987; Fox et al., 1987). Channels with similar although not identical properties have been found in rat sympathetic neurons and PC12 cells (Hirning et al., 1988; Plummer et al, 1989) and a large variety of central neurons (Regan et al., 1991). Within these preparations, N-type channels exhibit a set of characteristics that distinguish them from other voltage-dependent Ca^{2+} channels (e.g., T-, L-, and P-type). In general, N-type channels require relatively strong depolarizations for activation, but are prone to inactivate during pulses to weakly depolarized potentials; they are blocked by ω-conotoxin but not by dihydropyridines or ω-agatoxin IVA. Their unitary Ba^{2+} conductance is generally less than that of L-type channels but greater than T-type channels. A combination of these discriminatory parameters is usually sufficient to allow a reliable distinction between N-type and L-type or P-type channels (see Bean, 1989a; Hess, 1990; Tsien et al., 1991).

Less is known about the gating properties of N-type channels than L-type channels. Whole-cell recordings have provided information about N-type channel activation, inactivation, and pharmacology (e.g., Jones and Marks, 1989a,b). Unitary recordings have revealed variable inactivation rates of N-type channels (Plummer and Hess, 1991). However, no description of rapid activation kinetics is available at the level of single N-type channels.

Studies of rapid gating kinetics are particularly interesting because there have been repeated suggestions that N-type channels show more than one mode of gating. Shifts between "willing" and "reluctant" gating modes have been hypothesized to account for changes in voltage dependence of activation during norepinephrine inhibition (Bean, 1989b) and the relief of this

Received Mar. 26, 1992; revised July 10, 1992; accepted July 15, 1992.

We are grateful to Keith Bley and Pedro Rivas for their participation in early stages of this project, Ji-Fang Zhang for carrying out Monte Carlo simulations, Jian Yang for access to experimental data, and David Friel and Felix Schweizer for valuable assistance and advice on computer programs. We thank Richard Aldrich, Ruth Lagnado, and David Friel for helpful comments on the manuscript. This work was supported by an NRSA award (A.H.D.), a fellowship from the American Heart Association (D.L.), U.S. Public Health Service Grants NS24067 and HL13156 (R.W.T.), and a National Institutes of Mental Health Silvio Conte Center of Neuroscience Research (MH 48108).

Correspondence should be addressed to Richard W. Tsien at the above address.

[a] Present address: Department of Biology, University of Houston, Houston, TX 77204.

[b] Present address: Section of Physiology, Box GB302, Brown University, Providence, RI 02912.

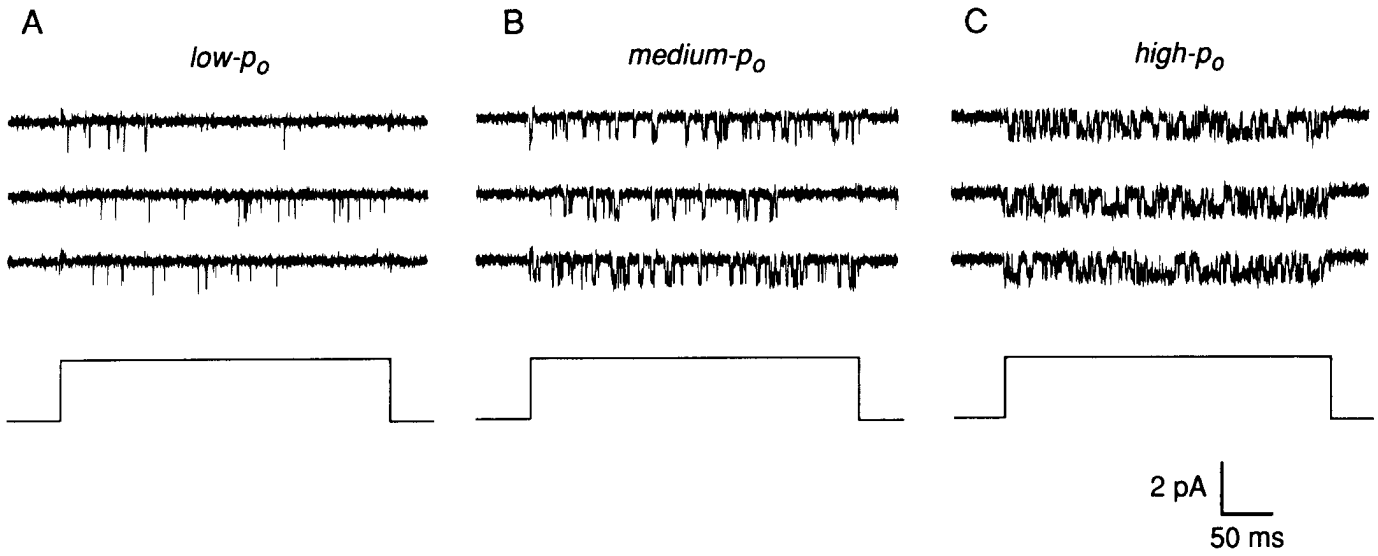

Figure 1. Multiple kinetic patterns of N-type calcium channel gating: leak-subtracted traces selected from a single-experiment to illustrate gating in the low-, medium-, and high-p_o modes. The voltage protocol, displayed at the *bottom* of each panel, was a depolarization from −80 mV to −10 mV. Experiment dl9c.

inhibition after strong depolarizing prepulses (Elmslie et al., 1990; Kasai, 1992). This modal scheme has also been invoked to explain calcium current facilitation (Ikeda, 1991). These hypotheses for N-type channels find some precedence in previous analysis of modes of gating of L-type channels (Hess et al., 1984; Nowycky et al., 1985b). Modal gating is inferred when a channel changes its kinetic behavior suddenly and maintains it for several seconds in the absence of a change in test potential and bathing solutions. In the case of L-type channels, shifts between gating modes occur during stimulation of Ca^{2+} currents by dihydropyridines (Hess et al., 1984), β-adrenergic agonists (Yue et al., 1990), and the activity-dependent Ca^{2+} channel potentiation (Pietrobon and Hess, 1990). Previous single-channel recordings of N-type channels suggested the presence of two distinct open states (Lipscombe et al., 1989). We have now used high-resolution single-channel analysis to establish whether N-type channels show discrete modes of gating and to determine the kinetic properties within each mode.

This article focuses on analysis of opening and closing kinetics of N-type channels in frog sympathetic neurons. This a particularly favorable system since the cells lack T-type channels, and N-type channels greatly outnumber L-type channels. We found that a single N-type channel can undergo spontaneous shifts between three gating modes, each with markedly different mean open and closed times at a fixed test potential and different voltage dependence. Typically, the channel remains in the same kinetic pattern for periods ranging from several seconds to minutes, a time scale several orders of magnitude slower than required for individual open–closed transitions. Interestingly, the unitary flux through the channel can be significantly larger when the channel is in the mode with the lowest open probability (p_o). The differences in kinetics and unitary conductance support the idea that modes reflect fundamentally different configurations of the channel.

Materials and Methods

Cell culture. Sympathetic neurons were dissociated from the entire sympathetic chains of adult bullfrogs (*Rana catesbeiana*) following the procedure of Lipscombe et al. (1988) and maintained in culture at 16°C or 23°C for up to 15 d. The cells were plated in noncoated plastic dishes (Corning) and supplemented with growth medium [73% L-15 medium (GIBCO), 7% Nu-Serum (Collaborative), 10 mM glucose, 1 mM $CaCl_2$, 100 U/ml penicillin, 100 mg/ml streptomycin]. After a few days, healthy cells developed processes that made contacts with each other.

Patch-clamp recordings. Single-channel measurements were made according to standard techniques (Hamill et al., 1981). The membrane potential was zeroed with the following bath solution: 140 mM K-aspartate, 10 mM EGTA, 10 mM glucose, 1 mM $MgCl_2$, 10 mM HEPES (pH adjusted to 7.3 with KOH). Pipettes contained solutions of 110 mM $BaCl_2$, 10 mM tetraethylammonium chloride (TEA-Cl), 5 mM 4-aminopyridine, and 5 mM HEPES (pH adjusted to 7.3 with TEA-OH), and had resistances of 7–15 MΩ. Current was recorded in the cell-attached configuration with an Axopatch-1C (Axon Instruments) and filtered at 2 kHz (8-pole Bessel filter, Frequency Devices). For most of the experiments, the membrane potential of the patch was held at −80 mV, but occasionally it was changed to −40 mV to identify N-type Ca channels through their voltage-induced inactivation. Command pulses of 312 msec in duration were delivered every 4 sec, and current was sampled every 100 μsec and stored on computer.

Data analysis. Data acquisition, analysis, and simulation were performed with 486-based microcomputers using AXOBASIC software. Leak and capacitative currents were subtracted from the traces using blank sweeps that were recorded at the same test potential and either averaged or fit by single exponential decays. Channel openings were detected with the half-amplitude criterion. For each sweep, $\langle t_o \rangle$ was calculated as the arithmetic average of all open times, and $\langle t_c \rangle$ as the average of all closed times excluding the first and last closures during the depolarization. The open probability, p_o, was calculated as $\langle t_o \rangle / (\langle t_o \rangle + \langle t_c \rangle)$. This is equivalent to the ratio of the total open time during the sweep to the time between the first opening and the completion of the last complete open–closed duty cycle, in which the last closure is assigned a value of $\langle t_c \rangle$. This procedure removes the influence of early inactivation on the estimation of p_o. Fits of amplitude histograms, open and closed time distributions, and voltage dependence of kinetic parameters were performed with the maximum likelihood algorithm using a Simplex routine (Kowalik and Osborn, 1968; Colquhoun and Sigworth, 1983).

In some experiments, we observed channel openings of much smaller size than those of typical N-type Ca^{2+} channels. These events might reflect a subconductance similar to that described for rat sympathetic neurons (Plummer et al., 1989). Such activity could always be clearly distinguished from typical N-type Ca channel behavior by virtue of its smaller slope conductance (8 pS) and the relatively negative position of its voltage-dependent activation curve. Sweeps that displayed this activity alone or in conjunction with typical N-type channel openings were excluded from the analysis presented here. In a few patches, this smaller conductance was found alone for the entirety of the experiment. It is unclear whether the subconductance represents another channel subtype or an infrequently occurring gating mode.

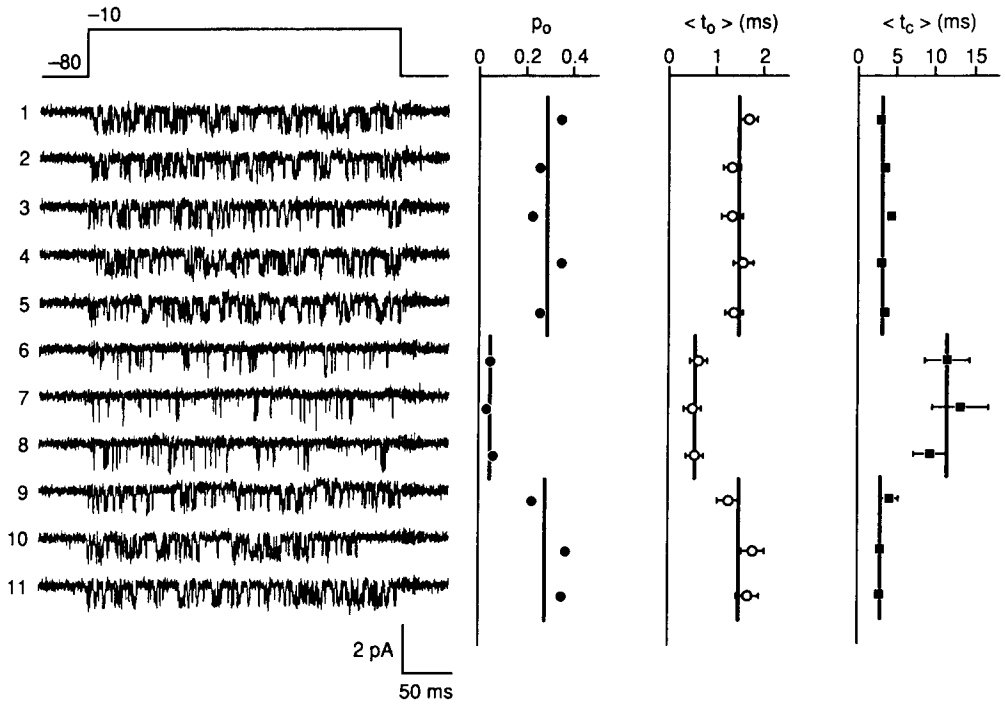

Figure 2. A single N-type channel alternates between the low- and medium-p_o modes. A run of consecutive leak-subtracted sweeps is displayed (*left*) together with corresponding sweep-by-sweep plots of open probability p_o, mean open time $\langle t_o \rangle$, and mean closed time $\langle t_c \rangle$ (arithmetic averages, ± SEM). p_o is calculated as $\langle t_o \rangle / (\langle t_o \rangle + \langle t_c \rangle)$ as described in Materials and Methods. Voltage protocol is shown as the top trace. Experiment dl9d.

Results

Different kinetic patterns

N-type Ca^{2+} channels display diverse patterns of opening and closing in response to repeated depolarizations to a fixed test potential. As an overview, Figure 1 illustrates recordings of unitary N-type openings that were evoked by 312 msec depolarizing pulses from −80 to −10 mV. Figure 1*A–C* shows sets of current records, selected to illustrate the different types of gating behavior, where only one channel appears to be active in any sweep. In Figure 1*A*, the kinetic pattern is characterized by brief openings separated by long closures and a low p_o. In Figure 1*C*, the openings are much longer and the closures much briefer, and consequently, p_o is relatively high. Figure 1*B* shows sweeps with openings and closures less extreme in duration than in either *A* or *C*, and an intermediate level of p_o (medium p_o). This kind of diversity in the kinetics of channel gating was seen, to various extents, in a large number of cell-attached patch recordings ($N > 50$).

The recording illustrated in Figure 1 was typical of most cell-attached patches in that it contained at least two channels, as judged by the occasional appearance of overlapping openings (not shown). Transitions among different gating patterns were observed even in patches containing only one functional channel (Figs. 2–4). Different patterns of gating are evident by visual inspection of the current records themselves and are further documented by analysis of p_o, mean open time $\langle t_o \rangle$, and mean

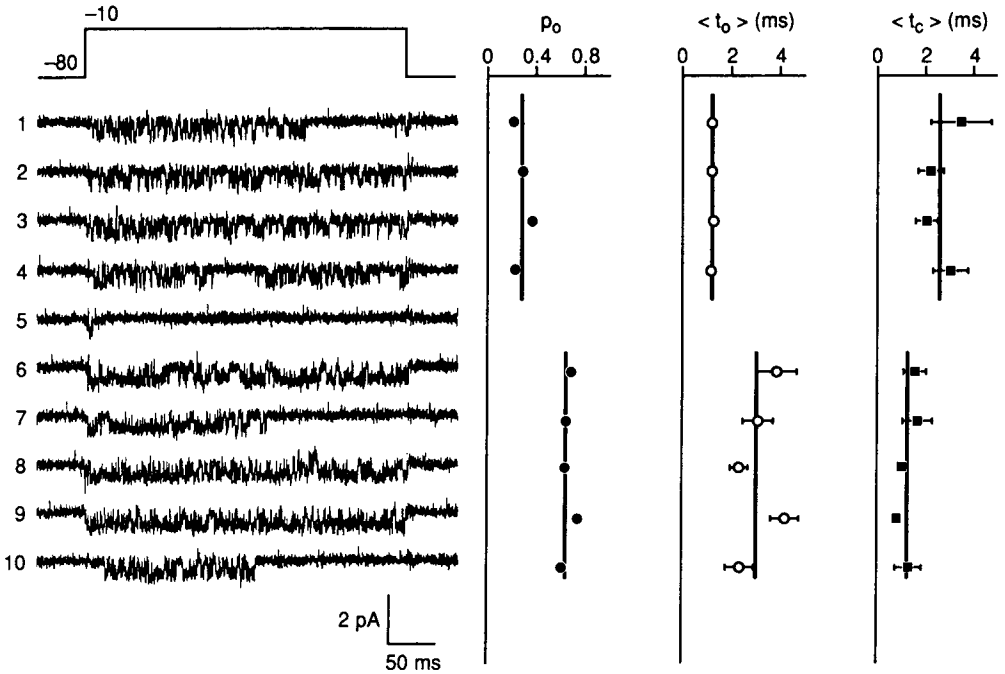

Figure 3. A single N-type channel shifts from the medium- to the high-p_o gating mode. Sweep-by-sweep plots of p_o, $\langle t_o \rangle$, and $\langle t_c \rangle$ are displayed adjacent to the corresponding sweep. p_o is calculated as in Figure 2. Experiment ada18.

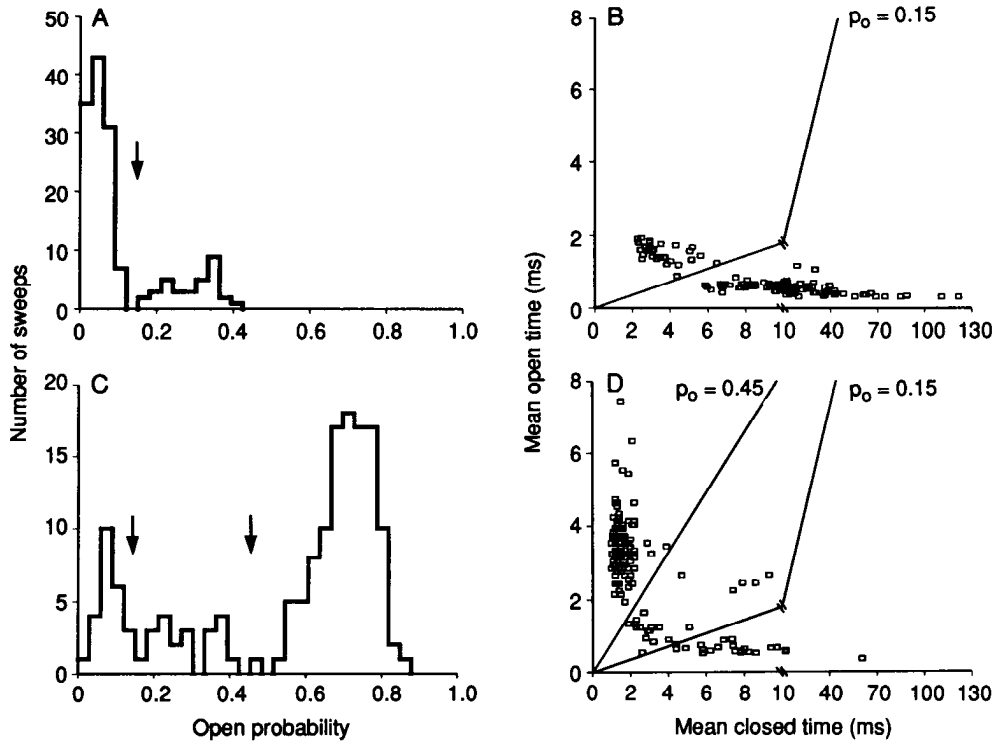

Figure 4. Overall kinetic behavior in two exemplar experiments. *A* and *B* show kinetic parameters determined for the experiment illustrated in Figure 2; *C* and *D*, for the experiment in Figure 3. *A* and *C*, Histograms of sweep p_o. The *ordinate* plots the number of sweeps per bin (bin width = 0.03). The *arrows* mark p_o values of 0.15 and 0.45, chosen as cutoffs to separate peaks of low-, medium-, and high-p_o behavior. *B* and *D*, Plots of $\langle t_o \rangle$ against $\langle t_c \rangle$. Each symbol represents $\langle t_o \rangle$ and $\langle t_c \rangle$ values determined for an individual sweep. Note that the *abscissa* plots time on a contracted scale beyond the break at 10 msec. In *B*, the *broken diagonal line* corresponds to $p_o = 0.15$. Note that this separates the sweeps into two distinct populations. *D* includes an additional diagonal line corresponding to $p_o = 0.45$, which lies below an additional cluster of data points corresponding to high-p_o gating. Between $p_o = 0.45$ and $p_o = 0.15$ are four data points representing sweeps with $\langle t_o \rangle \sim 2$ msec and $\langle t_c \rangle$ ranging from 6 to 10 msec. Although these sweeps fell in the category of "medium-p_o," they each showed a transition between the low- and high-p_o modes.

closed time $\langle t_c \rangle$. Distinctions between gating patterns of low p_o and medium p_o are illustrated in Figure 2. The pattern of gating appears relatively uniform up to the fifth sweep, with $p_o \sim 0.3$. In the next three sweeps, p_o falls approximately sixfold to ~0.05, but recovers abruptly to ~0.3 during the ninth sweep. The changes in channel p_o are the result of marked changes in both open and closed durations: more than a twofold difference in $\langle t_c \rangle$ and a nearly fourfold difference in $\langle t_o \rangle$. These records are representative of the gating behavior seen throughout the entire recording (~35 min). The vast majority of the changes in gating pattern took place during the interval between depolarizations, rather than during the pulses themselves (see Slow transitions between gating modes, below).

The distinction between gating patterns of medium-p_o and high-p_o activity is illustrated in Figure 3. These consecutive sweeps originate from another single N-type Ca^{2+} channel patch. Clear differences between the kinetic pattern of the first four sweeps and the last five sweeps are highlighted by the accompanying plots of p_o, $\langle t_o \rangle$, and $\langle t_c \rangle$. The first four sweeps show p_o values close to 0.3, similar to the values found for groups of sweeps in Figure 2. After a nearly blank record, the p_o shifts upward to a mean p_o of 0.6 during the sixth sweep. This change in p_o is paralleled by a doubling of $\langle t_o \rangle$ and a twofold decrease in $\langle t_c \rangle$.

Each of the data points for $\langle t_o \rangle$ and $\langle t_c \rangle$ in Figures 2 and 3 is associated with an SEM (in some cases the error bars are so small that they lie within the symbols). The apparent differences in mean open or closed durations between modes were found to be highly significant. For example, consider the estimates of $\langle t_o \rangle$ for medium- and high-p_o activity in Figure 3. The highest estimate of $\langle t_o \rangle$ in the medium-p_o records (sweep 3) was 1.32 ± 0.19 msec ($N = 92$), and the lowest value for $\langle t_o \rangle$ in the high-p_o traces (sweep 8) was 2.08 ± 0.28 msec ($N = 98$). The null hypothesis that both samples are drawn from the same parent distribution can be rejected at the $p < 0.05$ level (Student's t test). Estimates of $\langle t_c \rangle$ for the same sweeps (2.05 ± 0.31 and 1.05 ± 0.15) are different at the $p < 0.01$ level. Likewise, a comparison of $\langle t_c \rangle$ for low- and medium-p_o sweeps (e.g., sweeps 6 and 3 in Fig. 2) yielded qualitatively similar conclusions. While the number of open and closed events was smaller for low-p_o sweeps ($N \sim 35$), differences in $\langle t_o \rangle$ and $\langle t_c \rangle$ between these modes were nevertheless significant ($p < 0.05$, $p < 0.02$, respectively). The overall conclusion is that medium-p_o gating may be readily distinguished from either low-p_o or high-p_o activity by consideration of either $\langle t_o \rangle$ or $\langle t_c \rangle$.

This study was mainly directed at studying rapid transitions between closed and open states. However, it should be noted that variations in the rate of inactivation may also be seen. For example, in some of the traces in Figure 3, channel openings disappear well before the end of the depolarizing pulse. Evidently, single N-type channels in frog sympathetic neurons can spontaneously switch between relatively rapid inactivation and little or no inactivation (see Kongsamut et al., 1989), as previously reported in rat sympathetic neurons (Plummer and Hess, 1991). The variations in inactivation rate appear independent of modal changes in activation kinetics (see also Rittenhouse et al., 1991). For the purposes of studying rapid opening and closing kinetics, we minimized the influence of variable inactivation

kinetics by excluding from the kinetic analysis the last closed interval during a depolarizing pulse.

Classification of sweeps into groups

Data from the same single-channel patches were used to construct histograms showing distributions of sweep p_o (Fig. 4*A*,*C*). The distribution obtained from the experiment of Figure 2 shows two distinct peaks (Fig. 4*A*), corresponding to the two kinds of sweeps that were separated by visual inspection. This type of distribution was seen in less than 20% of the cells. Figure 4*C* shows the distribution of p_o for all the sweeps in the experiment of Figure 3. This histogram is dominated by a large peak centered around $p_o = 0.7$ that includes most of the sweeps in this experiment. The population of sweeps in the high-p_o mode stands apart from the rest of the distribution. The remainder of the sweeps appear in a well-defined peak centered around $p_o = 0.08$ (corresponding to the low-p_o peak in Fig. 4*A*), and a rather broad distribution of sweeps of intermediate p_o. p_o cutoffs of 0.15 and 0.45 (Fig. 4*A*,*C*, arrows) are chosen to separate sweeps of low-, medium-, and high-p_o behavior.

Another way of representing the nonhomogeneous gating behavior of the channel is to plot $\langle t_o \rangle$ against $\langle t_c \rangle$ on a sweep-by-sweep basis (Fig. 4*B*). In this case, a probability cutoff of 0.15 is represented by a diagonal through the origin. The data points below the diagonal (short $\langle t_o \rangle$, long $\langle t_c \rangle$) correspond to the group of sweeps with $p_o < 0.15$; the points above the diagonal represent sweeps with $p_o > 0.15$.

If one considers all the sweeps for $\langle t_c \rangle$ up to 10 msec, there is a clear negative correlation between $\langle t_o \rangle$ and $\langle t_c \rangle$: short openings appear to be strongly associated with long closures. This negative correlation is not consistent with a simple unbranched kinetic scheme. It can be accommodated by Markovian kinetics, but only if the scheme has a branched topology, with at least one closed state and one open state in each branch (Jackson et al., 1983; McManus and Magleby, 1989). However, if one considers separately the groups on either side of the $p_o = 0.15$ line, there is little or no correlation between $\langle t_o \rangle$ and $\langle t_c \rangle$ within each group. The kinetics within each group would therefore be consistent with a simple linear scheme comprised of a series of closed states leading up to a series of one or more open states (C . . . C-O-O . . .). For this kind of scheme, the closed times would be distributed independently of the length of the previous openings.

The populations of sweeps defined in Figure 4*C* were also examined in a plot of $\langle t_o \rangle$ versus $\langle t_c \rangle$ (Fig. 4*D*). Here, as in Figure 4*B*, the low-p_o sweeps are represented by a horizontal streak of data points below the $p_o = 0.15$ diagonal and the medium-p_o sweeps cluster together above this diagonal. The high-p_o peak is represented as an additional group of points, lying above the $p_o = 0.45$ diagonal, with $\langle t_c \rangle$ values consistently smaller than 2 msec and $\langle t_o \rangle$ values extending between 2 and 8 msec. This kind of behavior was completely absent in Figure 4*B*. Within the population of high-p_o points, there is no clear correlation between $\langle t_o \rangle$ and $\langle t_c \rangle$, suggesting once again that the kinetics within the mode can be accounted for by an unbranched series of states (see Simple and consistent gating kinetics within each mode, below). If medium-p_o and high-p_o sweeps were not separated, the scheme would have to be complicated enough to account for a clear negative correlation between $\langle t_o \rangle$ and $\langle t_c \rangle$.

Slow transitions between gating modes

As a general rule, channels displayed a mode of gating for several consecutive sweeps before changing spontaneously to another mode or becoming temporarily inactive. This clustering behavior was analyzed in several ways. One approach, illustrated for a representative experiment in Figure 5, tabulates the number of times that a sweep of a particular type was followed by a sweep of the same type or a different type. A total of 161 sweeps were classified in this way. The boldface number in each box represents the observed number of sweeps of each category, whereas the number in parentheses represents the expected number if each type of gating occurred randomly, independent of the previous history of gating. Examination of the entries on diagonal shows that the observed frequencies of repeats of the same kind of gating are considerably higher than expected if the pattern of gating varied randomly from one depolarization to the next. Analysis with χ^2 indicates that the observed frequencies are statistically different from the expected ones at a significance level of $P < 0.005$. A highly diagonalized contingency table was obtained in all four experiments for which this type of analysis was performed.

Sweep (k + 1)

Sweep k	blank	low	medium	high
blank	**18** (7)	**1** (4)	**1** (3)	**15** (20)
low	**1** (4)	**17** (2)	**2** (2)	**0** (11)
medium	**1** (3)	**1** (2)	**9** (2)	**4** (9)
high	**14** (19)	**0** (11)	**4** (9)	**73** (52)

Figure 5. N-type channels tend to display the same pattern of gating from one sweep to the next: contingency table of calcium channel gating from a single-channel patch (ada18). The gating pattern of sweep (k + 1) is shown in relation to gating of sweep k. The observed numbers of sweeps in each category are shown in *boldface*. The numbers expected for random occurrence are shown below in *parentheses*. These were calculated as the product of individual modal probabilities times the total number of sweeps.

A somewhat different but complementary approach is to subdivide a recording session into runs of sweeps showing the same pattern of gating. Analysis of the lengths of the runs provides direct information about how long a channel remains in a mode of gating before switching to another mode. We distinguished between runs of blank sweeps and of low-, medium-, and high-p_o modes. For the experiment documented in Figure 5, the mean numbers of records per run were 1.88 (blanks), 3.00 (low p_o), 1.43 (medium p_o), and 3.5 (high p_o). Given the 4 sec cycle time between sweeps, the mean sojourn in the individual gating modes was of the order of 8–15 sec.

Collected results from a total of four experiments were pooled to yield distributions of run lengths for each of the active modes and for sweeps with no detectable openings (Fig. 6). Each of the histograms is reasonably well fit by a single exponential curve, as expected if the exit rate from an individual mode obeys first-order kinetics as in a Markov model.

Simple and consistent gating kinetics within each mode

Separation of the sweeps into separate populations facilitates the analysis of gating kinetics. Figure 7 shows distributions of

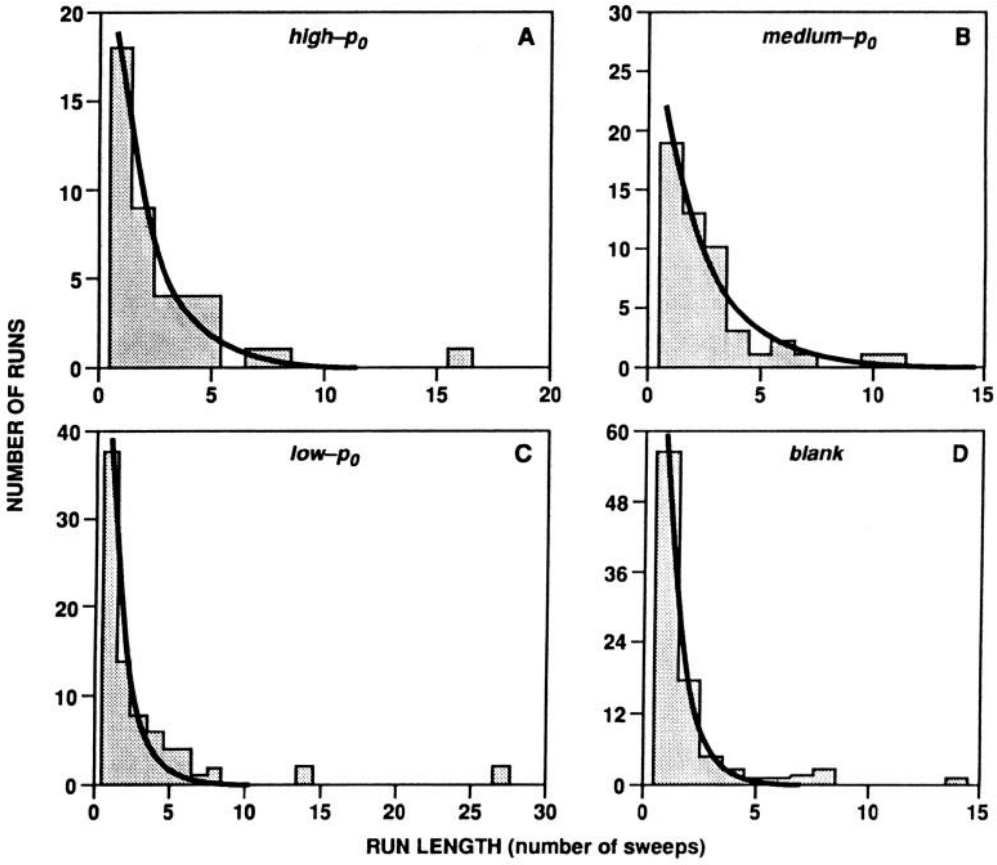

Figure 6. Distributions of run lengths for various modes. A run was defined as a series of consecutive sweeps displaying channel activity in the same mode. *A–C* show high-, medium-, and low-p_o modes, respectively. *D* displays run lengths for consecutive series of sweeps showing no detectable channel activity (blanks). The histograms were constructed by pooling data from four experiments. The duration of sojourns in various modes can be obtained by multiplying the number of sweeps by 4 sec, the cycle time of the depolarizations. The *smooth curves* show single exponential fits to the distributions, corresponding to time constants of 6.8 sec (high p_o), 8.4 sec (medium p_o), 5.2 sec (low p_o), and 3.5 sec (blanks).

channel open times at −10 mV for the two exemplar single-channel experiments (Fig. 4*A,C*). The leftmost panels show the open time histograms of *all* sweeps in each of the experiments. In both cases, the distribution is poorly fit by a single exponential, indicating the existence of more than one open state. However, single exponentials proved to be sufficient once the sweeps were broken down into groups according to the mode of gating. In Figure 7*A*, this was accomplished by subdividing the records into low- and medium-p_o groups. In Figure 7*B*, subdivision into three modes was necessary; merely removing high-p_o sweeps (the most clearly defined group in Fig. 4*C*) left a distribution of openings that could not be fit by a single exponential (analysis not shown). Further separation between medium- and low-p_o sweeps gave three distributions, each conforming to a single exponential. The time constants of the exponentials ranged from ~0.35 msec for the low-p_o mode to 3 msec for the high-p_o mode.

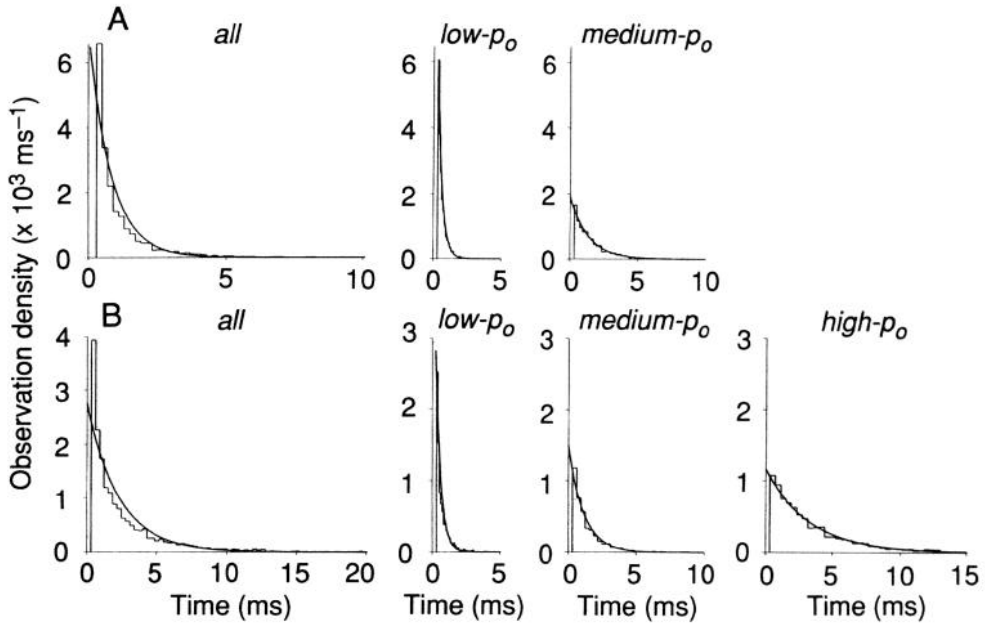

Figure 7. Separation of modal behavior simplifies analysis of open–closed kinetics: distributions of open times for all openings (left) and for individual modes (labeled *low*, *medium*, and *high*). *A*, Analysis of an experiment in which only low- and medium-p_o activity was observed (Fig. 4*A,B*; experiment dl9d). *B*, Analysis of experiment where all three modes were observed (Fig. 4*C,D*; experiment ada18). The *leftmost histograms*, made from all openings without modal classification, are poorly fitted by single exponentials. In contrast, histograms constructed from sweeps within the categories of low-, medium-, or high-p_o mode are fit very closely by single exponentials. Note that there is close agreement between the experiments in estimated values of exponential time constants. For *A* and *B*, respectively, τ_{low} = 0.32 and 0.40 msec; τ_{medium} = 1.3 and 1.2 msec. In *B*, τ_{high} is 3.1 msec. The relative proportion of detectable openings in each group were 67% (low) and 33% (medium) in *A* and 20% (low), 8% (medium), and 72% (high) in *B*.

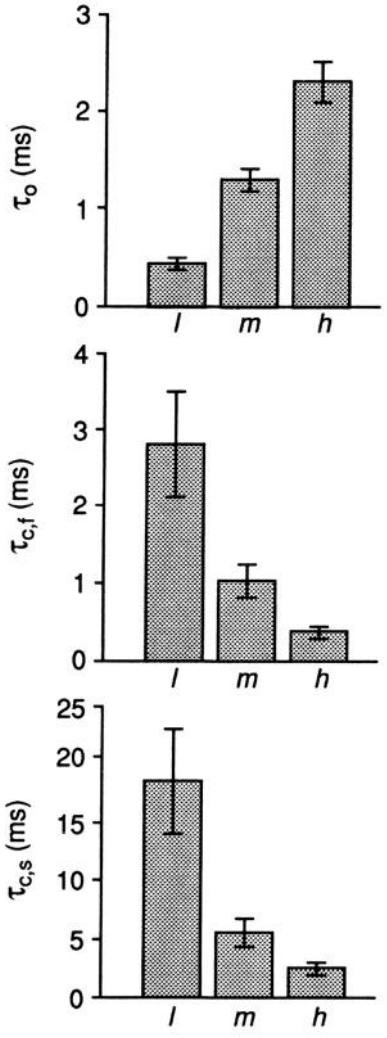

Figure 8. Mean values of open and closed time constants from 13 experiments. Data were collected from exponential fits of the open and closed time distributions after separating the sweeps into the low- (*l*), medium- (*m*), and high-p_o (*h*) modes on the basis of cutoffs at $p_o = 0.15$ and $p_o = 0.45$. $N = 7$ for low-p_o, and $N = 11$ for medium and high-p_o (the number of entries varies because some experiments displayed too few openings in a particular mode to allow a reliable fit of the distribution).

The relative areas under the individual distributions represent the relative proportion of openings within each mode (see Fig. 7 caption). These exemplar experiments illustrate the general finding that the proportion of time spent in each mode may vary widely from patch to patch. However, in all of our experiments, single exponentials provided good fits to the open time distributions within a mode.

A similar analysis of closed times was carried out after segregation of the sweeps into the three modes. For a given mode, fits to the distributions of closed times required at least two decaying exponentials. This kinetic behavior implies a minimum of two closed states. Thus, a minimal kinetic scheme within each mode can be stated as C2-C1-O, as found previously for activation kinetics of other types of voltage-gated Ca^{2+} channels (e.g., Fenwick et al., 1982; Reuter et al., 1982; Brum et al., 1984). Other schemes with more states but the same number of independent rate constants would work equally well (Shuba et al., 1991).

Figure 8 plots collected values of the exponential time constants for individual modes (13 experiments). The number of data points for each mode varies because some patches lacked enough sweeps within a particular mode to allow a reliable estimate of the open and closed time constants. The kinetic parameters for the high-p_o mode showed relatively little variation from one patch to the next, with an open time constant of about 2.4 msec and fast and slow closed time constants (τ_{cf}, τ_{cs}) of 0.4 and 2.5 msec. The medium-p_o mode displayed mean values of $\tau_o = 1.3$ msec, $\tau_{cf} = 1.0$ msec, and $\tau_{cs} = 6$ msec. Data for the low-p_o mode showed the greatest variability from patch to patch; mean values were $\tau_o = 0.4$, $\tau_{cf} = 2.8$, and $\tau_{cs} = 18$ msec.

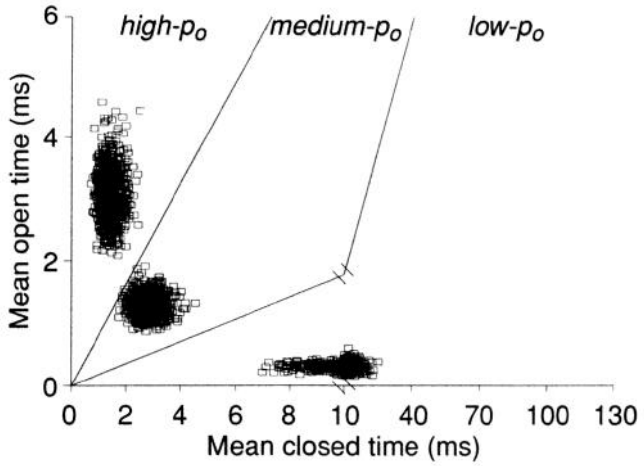

Figure 9. Monte Carlo simulation of kinetic behavior in individual modes: plot of $\langle t_o \rangle$ versus $\langle t_c \rangle$, for simulated sweeps, with 1000 simulated sweeps for each mode. Simulation was based on the kinetic scheme

$$\mathrm{C2} \underset{k_{-1}}{\overset{k_1}{\rightleftharpoons}} \mathrm{C1} \underset{k_{-2}}{\overset{k_2}{\rightleftharpoons}} \mathrm{O}$$

with rate constants (in units of sec^{-1}) for individual modes derived from experimental observations. High-p_o kinetics were obtained from analysis of the experiment in Figure 3. Kinetics of medium- and low-p_o modes were derived from the experiment of Figure 2. Values of k_1, k_{-1}, k_2, and k_{-2} were (in sec^{-1}), for high-p_o, 667, 1311, 2137, 324; for medium-p_o, 1378, 1033, 633, 769; and for low-p_o, 1163, 232, 104, 3125.

Monte Carlo simulation of modal analysis

As a check on whether this analysis can account for the general features of the kinetic behavior, Monte Carlo simulations of channel gating during depolarizing pulses were performed and analyzed by the same procedures used for real data (Fig. 9). The simulations used rate constants derived from analysis of the exemplar experiments, to allow a detailed comparison with Figure 4, *B* and *D*. These rate constants were derived according to standard equations (Fenwick et al., 1982) and are given in the Figure 9 caption. A thousand simulated sweeps were generated for each gating mode. When $\langle t_o \rangle$ is plotted against $\langle t_c \rangle$ for individual sweeps, the data points cluster in well-defined regions, separated by the p_o cutoffs of 0.15 and 0.45. The simulated points reproduce the overall shapes of the experimental clusters, and confirm that they can be reconstructed from three independent gating pathways, each characterized by its own set of rate constants.

The experimental data points are somewhat more scattered than the simulations. This may arise in a number of ways. If the N-type channel undergoes inactivation early during the depolarization, there will be a relatively small number of open and closed time intervals, and therefore a larger variation in $\langle t_o \rangle$

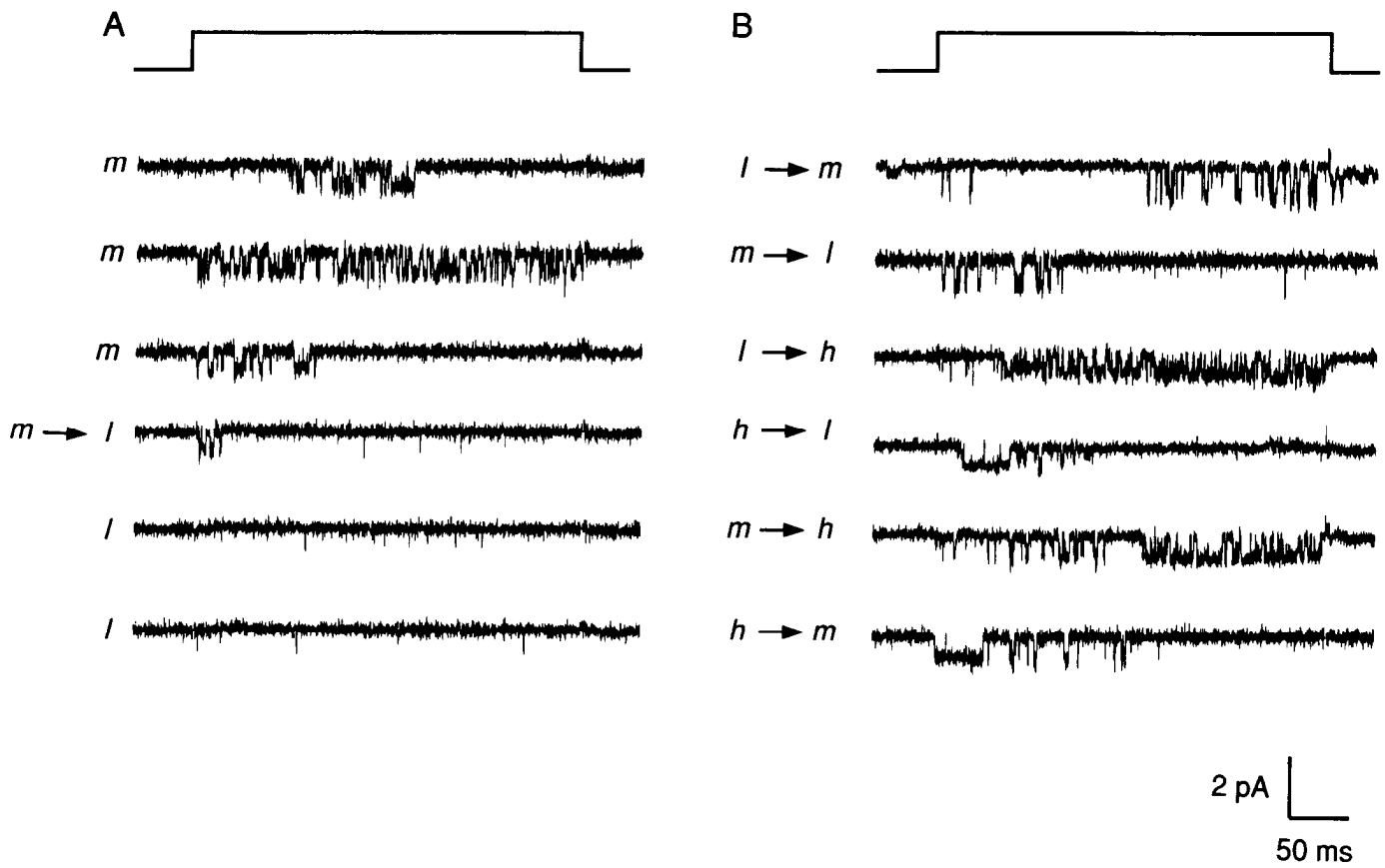

Figure 10. *A*, Consecutive traces showing a single modal transition (during *sweep 4*). The gating pattern was characteristic of the medium-p_o mode (*m*) during the preceding 11 sweeps (including *sweeps 1–3*), and remained as low p_o (*l*) for 9 sweeps after sweep 4 (including *sweeps 5* and *6*). *B*, Examples of apparent mid-sweep transitions between gating modes. The labels denote our classification of the modal transition. Leak-subtracted sweeps were selected from four experiments. The voltage protocol is shown at the *top* of *A* and *B*. The test potential was −10 mV in all cases, and the holding potential was either −80 mV or −70 mV.

and $\langle t_c \rangle$ in the experiment than in the simulation, which ignores inactivation. Likewise, transitions into and out of the inactivated state may occur during experimental depolarizations, but are not modeled in the simulation. Channels may exhibit additional modes, beyond the three considered here (see Discussion). Yet another possibility is that modal transitions may occur partway through the depolarizing pulse.

Modal transitions within individual sweeps

Some examples of mid-sweep modal transitions are presented in Figure 10, where *A* shows a sequence of consecutive records of N-type channel gating. During the first three sweeps, the gating pattern is typical of the medium-p_o mode (with rather variable inactivation); the gating changes abruptly to the low-p_o mode partway along sweep 4 and remains so thereafter. Figure 10*B* provides examples of intermodal transitions encompassing all possible permutations of modes, including low→medium, low→high, and so on. These records were classified by measuring p_o and $\langle t_o \rangle$ over time intervals of homogeneous gating as judged by visual inspection. There was no obvious indication of a graded change in gating properties; the transition seemed to be abrupt.

It was not unusual to find several such transitions in experimental recordings containing hundreds of sweeps. This is roughly as expected if the rate of switching between modes did not depend very strongly on membrane potential over the range between −80 mV and −10 mV. Since the single-channel recordings were carried out with 312 msec test depolarizations every 4 sec, most of the transitions would be expected to occur during the 3.7 sec interval between pulses. The percentage of transitions expected during the depolarizations themselves can be calculated as follows. For a switching rate of ~0.1 sec^{-1}, the likelihood of a transition amidst the depolarization would be (0.3 sec)(0.1 sec^{-1}) = 0.03 per pulse. This is comparable to the frequency of midsweep modal transitions we were able to detect. For example, some of the stray points in the $\langle t_o \rangle$–$\langle t_c \rangle$ plot in Figure 4*D* can be accounted for by intrasweep transitions (see Fig. 4 caption for details). In general, the rate of occurrence of such transitions was low enough not to hamper seriously the analysis of gating kinetics on a sweep-by-sweep basis.

Low-p_o openings can show larger unitary amplitude

It is interesting to compare the voltage dependence of the unitary current within each mode. No difference is seen in the current amplitude of openings in the medium- and high-p_o modes. However, the channel can show a larger unitary current amplitude in low-p_o sweeps than in the medium-p_o or high-p_o sweeps. This can be seen in Figure 2 and is illustrated further by the records in Figure 11. The broken lines represent an estimate of the open levels in a group of medium-p_o sweeps (Fig. 11*A*) and in a group of low-p_o sweeps (Fig. 11*B*), all at −10 mV test potential. There is a consistent difference in unitary current amplitude: when openings in low-p_o sweeps are clearly resolved, they attain values ~0.2 pA greater than unitary openings in the medium-p_o sweeps. The difference is reproducible, and opposite of that expected

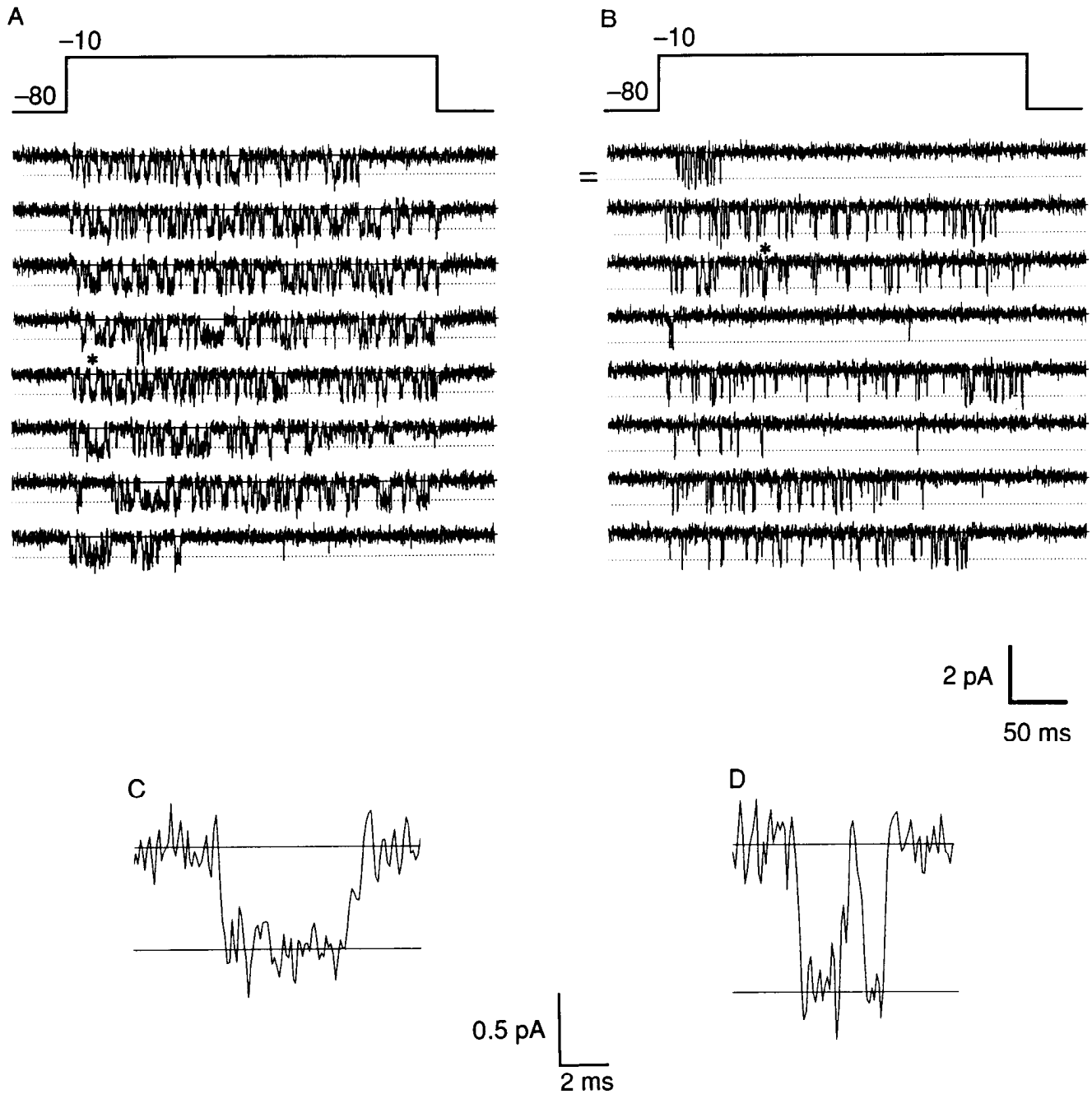

Figure 11. The single-channel conductance of the low-p_o mode can differ from that of the other modes: selected leak-subtracted sweeps illustrating medium-p_o gating (*A, C*) and the low-p_o gating (*B, D*). *C* and *D* are selected channel openings taken from records in *A* and *B* as indicated by the *asterisks*, displayed on an expanded time scale to highlight the difference in current amplitude.

for imperfect resolution of brief openings due to bandwidth limitations. Indeed, when records are expanded along the time axis (Fig. 11*C,D*), it is evident that many of the low-p_o openings are quite well resolved.

As illustrated in Figure 12*A*, the difference in unitary current is also apparent in all-points histograms of the current signal from the sweeps in Figure 11. The open channel current levels correspond to peaks of Gaussian distributions (arrows) of −0.72 pA for the medium-p_o mode and −0.95 pA for the low-p_o mode. Differences between the unitary current amplitude of the low-p_o mode and medium/high-p_o modes were found consistently over a range of membrane potentials. Figure 12*B* shows collected results from six patches. The unitary current amplitude for sweeps showing low-p_o gating is at least 0.2 pA larger than the corresponding values for high- and medium-p_o sweeps at several test potentials. The single-channel conductance was found to be ~18 pS for both modes. While the $i(V)$ relations run parallel over a considerable range of potentials studied, it seems possible that the $i(V)$ curves would converge at strongly positive potentials.

The low-p_o openings are themselves considerably smaller in unitary current amplitude than openings of L-type channels (~1.2–1.3 pA at −10 mV). L-type channels may also be distinguished by their resistance to inactivation by steady depo-

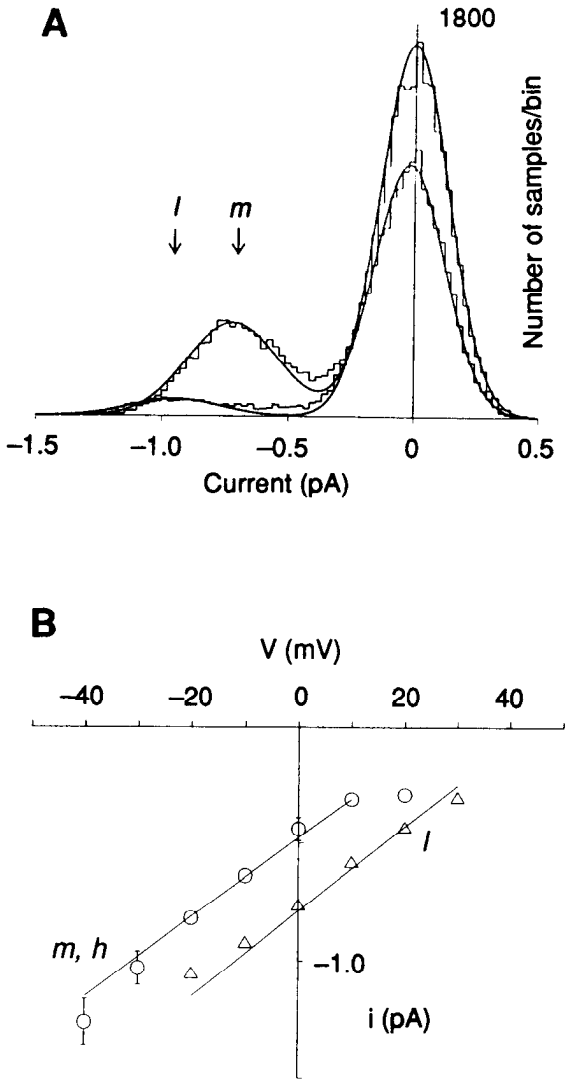

Figure 12. *A*, Amplitude histograms of the sweeps in Figure 11. The closed and open current levels were fitted individually by single Gaussian distributions; the sum of the fitted Gaussians is displayed. The peaks of the current amplitudes are marked by the *arrows* (*l*, low p_o; *m*, medium p_o). *B*, Unitary current–voltage relationships for low-p_o behavior (△) and medium/high-p_o behavior (○). The current amplitude was averaged for a number of sweeps in each of five experiments, but the lines were drawn from the regression analysis performed with the individual experimental values. Single-channel current amplitudes of medium- and high-p_o sweeps were grouped together since they showed no apparent difference. Both regression lines have slopes of 18 pS. The y-intercepts are −0.49 pA for the medium/high-p_o modes and −0.80 pA for the low-p_o mode.

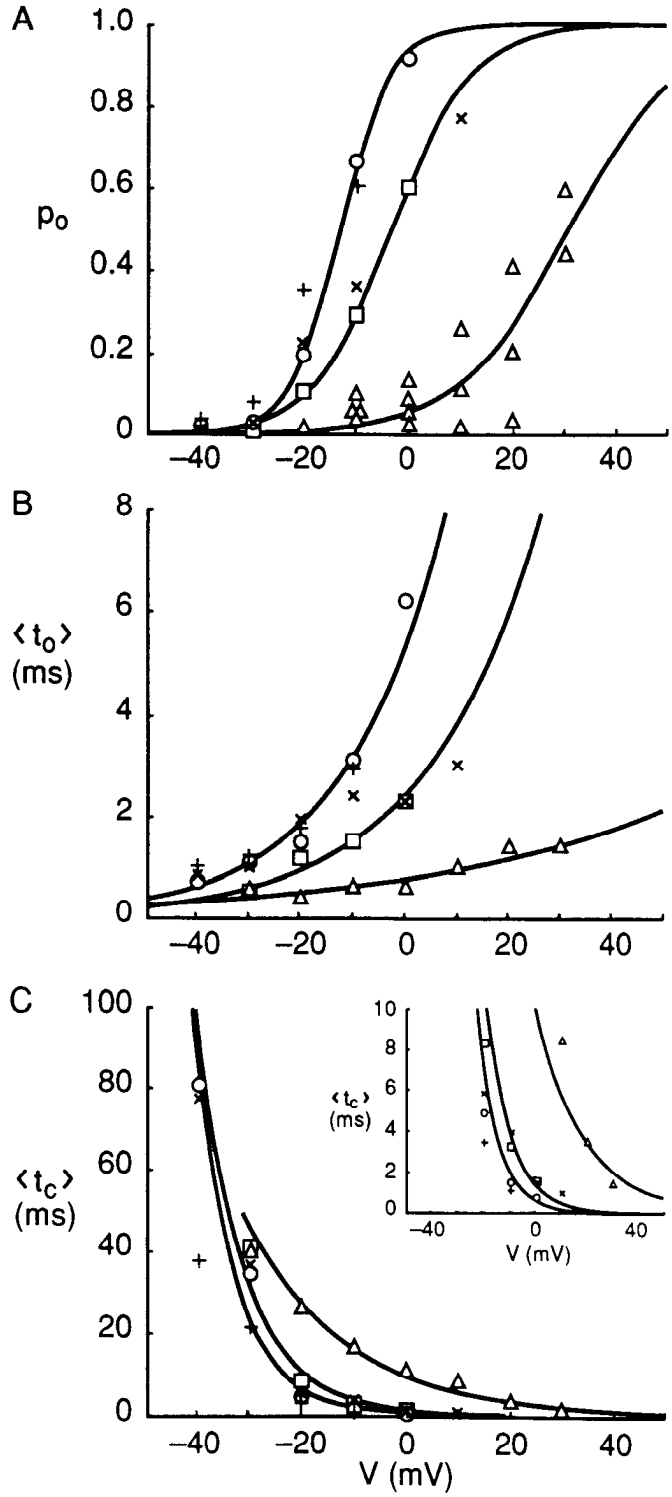

→

Figure 13. Voltage dependence of kinetic parameters. *A*, Open probability, $p_o(V)$. The data points of the low-p_o mode (△) were collected from seven patches, four of which containing a single channel. For the other patches, which had two channels, we mostly chose for analysis sweeps where only one channel was active. In some cases, however, we analyzed some sweeps that clearly displayed the continuous activity of both channels, and in those cases the aggregate opening probability was divided by 2. Boltzmann curves of the form $p_o(V) = [1 + \exp\{-(V - V_{1/2})/k\}]^{-1}$ were fitted to these low-p_o data ($V_{1/2}$ = 31 mV; k = 11 mV), and those pertaining to the medium-p_o mode (□; $V_{1/2}$ = −3.2 mV; k = 7.8 mV) and the high-p_o mode (○; $V_{1/2}$ = −13.2 mV; k = 5 mV). Also plotted for the sake of completeness are data from two other experiments (+ and ×) in which medium- and high-p_o were not clearly separated. Although the curve fitting was performed without regard for these points, it is clear that they fall in the range of the curves for medium and high p_o. *B*, Voltage dependence of the mean open times. *Symbols* are as in *A*, except that the data for the low-p_o mode have been averaged. The *solid lines* represent the exponential fits of the data done by linear regression of data plotted on a logarithmic scale. An *e*-fold change in $\langle t_o \rangle$ is obtained for 50, 22, and 19 mV for the low-, medium-, and high-p_o modes, respectively. *C*, Voltage dependence of the mean closed times. *Symbols* are as in *B*. The *solid lines* represent the exponential fits (linear regression of a logarithmic plot). An *e*-fold change in $\langle t_c \rangle$ is obtained for 19, 9.3, and 8 mV for the low-, medium-, and high-p_o modes, respectively. The *inset* shows $\langle t_c \rangle$ plotted on a vertically expanded scale.

larizations. We routinely applied steady depolarizations to −40 mV to verify that channel activity inactivated as expected for N-type Ca^{2+} channels (but not L-type channels).

Differences in voltage-dependent activation

Figure 13 compares the voltage dependence of activation of the three modes. Figure 13*A* shows individual p_o values for low-p_o activity from seven experiments (triangles). Three of these patches exhibited low-p_o activity exclusively as judged by intermittent trials at −10 mV. In the other patches, low-p_o gating was isolated by a combination of characteristics, including unitary amplitude and gating kinetics, which make it appear quite different from the other modes over a wide range of potentials. Average values for $\langle t_o \rangle$ and $\langle t_c \rangle$ in the low-p_o mode were derived from the same set of experiments and are plotted in Figure 13, *B* and *C*.

It was harder to separate medium- and high-p_o activity at potentials beyond −10 mV because the p_o increases so strongly in both modes. The analysis of $p_o(V)$ for these modes (Fig. 13*A*) relied heavily on two individual experiments containing long runs with exclusively medium-p_o gating (squares) or high-p_o gating (circles). The plot also includes data from two other experiments (represented by + and ×) where it was more difficult to make a clear-cut distinction between medium- and high-p_o gating at voltages other than −10 mV. These data are included because they provide some information about the behavior of non-low-p_o gating in aggregate.

Data for $p_o(V)$ were fit with a function derived from the Boltzmann distribution (Fig. 13*A*). The $p_o(V)$ curves differed in their midpoints ($V_{½}$ = −13.2, −3.2, and 31 mV) and Boltzmann slope factors (k = 5, 7.8, and 11 mV) for high-, medium-, and low-p_o modes, respectively. Thus, there was a systematic progression in the position and steepness of the $p_o(V)$ relationships. The voltage dependence of the low-p_o mode shows a relatively large separation from the other two modes, which fall fairly close to each other along the voltage axis.

The voltage dependence of the mean open times and mean closed times for each mode were fit with simple exponential functions (Fig. 13*B,C*). In the low-p_o mode, $\langle t_o \rangle$ and $\langle t_c \rangle$ both displayed a shallower voltage dependence (e-fold slope factors of 50 mV and 19 mV, respectively) than in the other two modes (slope factors of ~20 mV and ~8 mV).

Discussion

This study provides direct evidence for the existence of multiple modes of N-type Ca^{2+} channel activation gating and a quantitative description of the open–closed kinetics within each mode. Our analysis at the level of unitary currents complements previous studies of whole-cell N-type currents that originally suggested the existence of "reluctant" and "willing" gating modes with different voltage dependence (Bean, 1989b; see also Elmslie et al., 1990; Ikeda, 1991; Kasai, 1992). We found that N-type channels exhibit at least three discrete patterns of gating, denoted as low-, medium-, and high-p_o modes according to their probability of being in the open state at −10 mV, a test potential where the different modes are particularly well resolved. The modes differ in the position and steepness of their voltage-dependent activation curves. Within each mode, the kinetics of gating were adequately described by a set of Markov states arranged in the same configuration (C2-C1-O) as found in kinetic studies of other types of Ca^{2+} channels (e.g., Fenwick et al., 1982; Reuter et al., 1982; Brum et al., 1984). The rate constants connecting these states are markedly different from

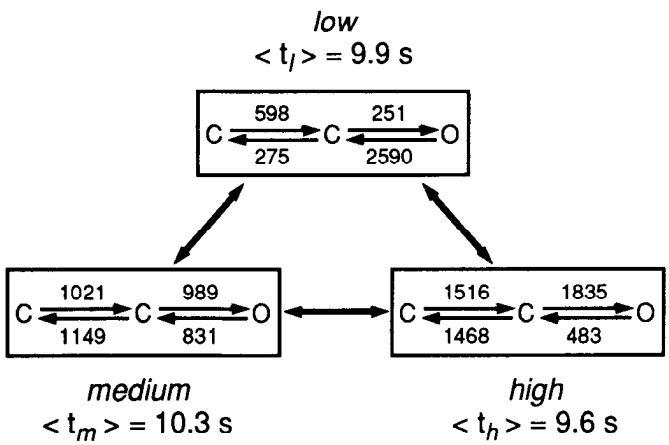

Figure 14. Summary of collected data on kinetic properties of the three modes. This scheme represents three sets of C2-C1-O states, corresponding to each mode, in equilibrium with each other. The mean dwell times in each mode are indicated as $\langle t_l \rangle$, and so on, and were derived from the experimental data in Figure 6*A–C*. The rate constants (in sec^{-1}) for the transitions between closed and open states are arithmetic averages of individual values from 13 experiments. For each experiment, the rate constants were calculated from estimates of the average p_o and of the areas and time constants of the exponential components of the open and closed time distributions (Fenwick et al., 1982).

one group of C2-C1-O states to the next (Fig. 14), thereby giving each mode its own distinctive kinetic signature.

Runs analysis demonstrated that N-type Ca^{2+} channels undergo spontaneous but infrequent transitions between the various patterns of gating. The average dwell time in any individual mode is ~10 sec, of the order of 10^3 to 10^4 times greater than mean durations of individual openings or closings within each mode. Thus, an N-type channel undergoes hundreds or thousands of open–closed transitions during a sojourn in a particular mode before spontaneously switching to a different gating pattern in another mode. Most transitions between modes occurred during the 3.7 sec interval between depolarizations, although mid-sweep transitions were also observed (Fig. 10). All permutations of transitions have been observed, and there was no clear indication for preferred transitions among the active gating modes.

Key discriminators between gating modes of N-type channels

The combination of high-, medium-, and low-p_o modes is more complex than the modal schemes proposed on the basis of whole-cell recordings. Are three modes really necessary? This amounts to asking whether the medium-p_o mode can be adequately discriminated from low-p_o behavior on one hand and the high-p_o mode on the other.

Medium- and high-p_o modes were readily separated on the basis of their kinetic behavior. The p_o values at −10 mV for medium- and high-p_o modes are ~0.3 and ~0.6, respectively. In either case, there are typically scores of open and closed events during a 320 msec depolarizing pulse. Thus, estimates of $\langle t_o \rangle$ and $\langle t_c \rangle$ for a given depolarization represent information about kinetic behavior that has already been signal averaged over the large number of events in that particular sweep. Each mean value carries with it an estimate of SEM (Fig. 3), so differences in mean values can be evaluated for statistical significance by conventional tests. In practice, medium- and high-p_o modes differ significantly with respect to both $\langle t_o \rangle$ and $\langle t_c \rangle$.

The relative proportion of sweeps displaying high-p_o gating is

quite variable. In some patches, sweeps with high p_o are in the majority (Fig. 4*C*), whereas in other cases, high-p_o gating can be completely absent (Fig. 4*A*). The variability is convenient for the purposes of isolating high-p_o gating as a distinct mode.

Medium- and low-p_o gating were also separated by comparing mean open or closed dwell times, calculated for individual sweeps. Plots of $\langle t_o \rangle$ against $\langle t_c \rangle$ provided a rather clear separation of sweeps into two populations. The mean closed time was the most dramatic discriminator, being about fourfold longer for low-p_o than for medium-p_o gating.

The amplitude of single-channel currents was an additional discriminator. When well resolved, the unitary amplitude of low-p_o openings was about 0.2 pA larger than medium- or high-p_o openings (Figs. 11, 12). It is important to note that the observed difference in conductance is contrary to that expected from bandwidth limitations, which would tend to make brief openings appear smaller.

The overall conclusion is that the medium-p_o mode can be adequately distinguished from high- or low-p_o behavior, supporting the use of a minimum of three active modes to describe N-type channel gating.

Is the modal scheme too simple?

The possibility remains that further subdivision of the rapid gating modes will eventually become necessary. This seems unlikely for the high-p_o mode because the open–closed characteristics are thoroughly documented and conform so closely to a conventional C2-C1-O scheme. Subdivision of low-p_o seems much more likely. Indeed, there is a wide variability in $\langle t_c \rangle$ values among different single-channel patches that exceeds what might be expected from random sampling from a single homogeneous distribution (e.g., Fig. 4*B,D*).

Sweeps classified as medium-p_o also show a wider spread on $\langle t_o \rangle$–$\langle t_c \rangle$ plots than expected from Monte Carlo simulations based on empirically derived C2-C1-O kinetics (Fig. 9). Some of the spread can be explained in terms of errors arising from sweep-by-sweep analysis. When transitions between various modes occur partway through a sweep, it is likely that the sweep will have an intermediate value of p_o and thereby be categorized (inappropriately) as medium p_o. In many cases, the misclassified sweep can be identified as an aberrant data point on the $\langle t_o \rangle$–$\langle t_c \rangle$ plot, with verification by visual inspection of the trace (see Fig. 4 caption). However, the midsweep transitions are not always obvious, so no attempt was made to exclude hybrid sweeps.

An additional subclass of medium-p_o gating may eventually be necessary to accommodate a pattern of activity characterized by brief openings (~1 msec) and brief closings (~1.5 msec). We referred to this as the "buzz mode," by analogy to a very rare pattern of activity of Ca^{2+}-activated K^+ channels (McManus and Magleby, 1988). The p_o is ~0.4, in the same range as the usual medium-p_o gating, although the closed times are much shorter. This kind of behavior was found infrequently (in less than 10% of the patches), so no attempt was made to isolate it from more typical medium-p_o behavior illustrated in Figure 4.

Comparison with modal analysis of other types of channels

Spontaneous changes in the pattern of gating have now been found for many kinds of channels. These include ligand-gated channels for glutamate (Patlak et al., 1979) and GABA (Macdonald and Twyman, 1991) as well as voltage-gated channels such as Na channels (Patlak and Ortiz, 1986; Nilius, 1988; Moorman et al., 1990; Zhou et al., 1991) and Ca^{2+}-activated K^+ channels (Moczydlowski and Latorre, 1983; McManus and Magleby, 1988). Modal changes in both activation and inactivation kinetics have been reported. The inactivation gating modes found for Na channels (Patlak and Ortiz, 1986; Nilius, 1988; Moorman et al., 1990; Zhou et al., 1991) are somewhat similar to those found for N-type Ca^{2+} channels (Plummer and Hess, 1991; see Different Kinetic Patterns, above).

The gating behavior described in this article finds strongest analogies with modal gating of L-type channels, previously described in heart cells (Reuter et al., 1982; Hess et al., 1984; Mazzanti and DeFelice, 1990; Yue et al., 1990) and neurons (Nowycky et al., 1985b). For L-type channels, as in the present case, modes were used as a way of describing well-defined patterns of rapid gating that remained stationary over a large number of duty cycles of opening and closing. L-type channels display three active modes, termed mode 0_a, mode 1, and mode 2 (Hess et al., 1984; Yue et al., 1990). In a qualitative way, these are analogous to low-, medium-, and high-p_o modes of N-type channels. Note however, that L-type mode 2 shows much longer openings ($\tau \sim 20$ msec near 0 mV) and much slower deactivation ($\tau \sim 10$ msec near -40 mV) than N-type high-p_o. The most striking contrast is in the frequency of occurrence of the modal behavior under basal conditions. L-type mode 2 is relatively rarely expressed (in perhaps 0.1–1% of depolarizations; Hess et al., 1984; Mazzanti and DeFelice, 1990), while high-p_o gating of N-type channels can appear in a majority of sweeps (Fig. 4*C*). The likelihood of an L-type channel visiting mode 2 is greatly increased by β-adrenergic stimulation acting through cAMP-dependent protein kinase. The prevailing hypothesis is that channel phosphorylation favors mode 2, just as depolarization promotes transitions between closed states and an open state (Yue et al., 1990). Put in more general terms, a mode may be viewed as an expression of a modulatory state of the channel, superimposed on the set of conformational states occupied during normal gating.

Modal switching can be regulated by membrane potential as well as hormones or neurotransmitters. Strong depolarizations promote transitions of L-type channels from mode 1 to mode 2 (Hoshi and Smith, 1987; Lee, 1987; Pietrobon and Hess, 1990; Artalejo et al., 1991). Facilitation of N-type currents has also been found in whole-cell recordings (Elmslie et al., 1990; Ikeda, 1991). More experiments are needed to see if strong depolarizations favor switching among rapid gating modes of single N-type channels.

Impact of modal weighting on divalent cation entry

Alterations in the proportion of time spent in the individual modes will strongly influence the functional contribution of N-type channels to divalent cation entry. The total current can be expressed as the sum of currents generated by the individual modes, whose contribution varies with its modal weighting coefficient (A_{low}, etc.):

$$I_{total} = I_{low} + I_{med} + I_{high}$$

$$I_{total} = A_{low} \cdot p_{o,low} \cdot i_{low} + A_{med} \cdot p_{o,med} \cdot i_{med} + A_{high} \cdot p_{o,high} \cdot i_{high}$$

Consider the case of a depolarization to a fixed potential, for example, -10 mV. The mean current in a high-p_o sweep is $p_{o,high} \cdot i_{high} = (0.65)(0.6\ pA) = 0.4$ pA, while the current in a low-p_o sweep is $(0.05)(0.8) = 0.04$ pA, an order of magnitude less. Thus, shifts from high-p_o to low-p_o gating would greatly reduce the overall Ca^{2+} entry during a voltage-clamp pulse or a high-K^+ depolarization.

Our experiments show a large degree of spontaneous variability from patch to patch in the modal weighting coefficients (A_{low}, etc.). This variability is interesting in light of previously reported differences in voltage-dependent activation curves derived from whole-cell tail current recordings (Bean, 1989b; Ikeda, 1991). Tail current activation curves based on our analysis of unitary N-type channel activity (data not shown) can be compared with published data from whole-cell recordings. A reconstructed activation curve based on the modal weights observed in a patch where high-p_o behavior is dominant (Fig. 4*D*) closely resembles the control curve in frog sensory neurons (Bean, 1989b) or the behavior of rat sympathetic neurons dialyzed with GDP-β-S (Ikeda, 1991). Conversely, the experiment of Figure 4*B*, which displays a majority of low-p_o behavior, yields a simulated activation curve similar to data for rat sympathetic neurons dialyzed with 0.5 mM GTP-γ-S (Ikeda, 1991). Evidently, activation of G-proteins favors low-p_o (reluctant) modal gating. One possible implication for our experiments is that the state of G-proteins or some other modulatory factor may vary widely from patch to patch or cell to cell even without the overt interventions used by Ikeda (1991).

Variability in the contribution of different modes has additional implications for identification of various Ca^{2+} current components in whole-cell recordings. Separation of N-type and L-type current components on the basis of voltage dependence of activation may be difficult if modal weighting is undetermined.

Molecular and functional implications

Taken together, these results support the idea that G-proteins influence the equilibrium between gating modes (Bean, 1989b; Elmslie et al., 1990; Ikeda, 1991; Kasai, 1992). How might this occur? (1) Our results demonstrate that the activity of individual channels is not controlled in an all-or-nothing manner, but can display multiple levels of p_o. This suggests that the G-protein does not merely block the channel. (2) The finding of at least three active modes of gating is also relevant to questions of mechanism. It does not support the simple hypothesis whereby binding of a single G-protein molecule is tightly linked to a transition from willing to reluctant gating. Other possibilities remain open. For example, one-to-one binding of a G-protein to an N-type channel might tilt the equilibrium between modes in favor of medium- and low-p_o behavior. Alternatively, more than one G-protein may bind to a channel, and modal changes may be determined by the number of G-proteins bound (see Kurachi et al., 1990; Karschin et al., 1991). (3) Gating kinetics within each of the modes can be adequately described by a common kinetic scheme (C2-C1-O). This suggests that gating in any mode arises from a common set of molecular conformations. (4) Switching between modes is relatively infrequent under the conditions of our experiments. This suggests that additional conformational changes in the channel, caused or favored by binding of G-protein(s), occur on a slow time scale to alter the energetics of the C2, C1, or O states. Under basal conditions, in the absence of neurotransmitter, the level of G-protein activation may be low enough to allow relatively long sojourns in high- or medium-p_o mode. (5) The $p(V)$ relations for the various modes are not related to each other by a simple shift along the voltage axis, but also exhibit differences in steepness (Fig. 13). This implies that the modulatory action is not just a simple electrostatic effect, as in the case of phosphorylation of K^+ channels (Perozo and Bezanilla, 1990). (6) The low-p_o mode often displays a significantly larger single-channel conductance than the other modes, suggesting the modulatory mechanism can somehow alter the aspects of the channel molecule that control ion permeation as well as opening and closing.

Whatever the details of the mechanism, the possibility of G-protein–driven changes in mode offers wide latitude for neurotransmitter-dependent modulation. Alterations in the weighting of modes has been hypothesized as a mechanism of neurotransmitter-driven downmodulation (Bean, 1989b). We have direct evidence for this in the case of modulation by norepinephrine (Delcour et al., 1992).

Shifts between gating modes are a more subtle kind of modulation than simply blocking or unblocking the channel. The ~40 mV shift in voltage dependence between high-p_o and low-p_o gating strongly reduces p_o at ~0 mV. However, it is important to recognize that even in low-p_o, open probability reaches a value of 0.5 at +30 mV, near the peak of an action potential. Thus, the impact of the modulation will depend greatly on the pattern of electrical activity (Elmslie et al., 1990; Kasai, 1992; cf. Penington et al., 1991). Relief of inhibition could take place by accentuation of depolarization, favoring channel opening within the low-p_o mode (Kasai, 1991), as well as by transitions from low-p_o to medium- or high-p_o modes (Bean, 1989b).

References

Aosaki T, Kasai H (1987) Characterization of two kinds of high-voltage-activated Ca-channel currents in chick sensory neurons: differential sensitivity to dihydropyridines and ω-conotoxin GVIA. Pfluegers Arch 414:150–156.

Artalejo CR, Dahmer MK, Perlman RL, Fox AP (1991) Two types of Ca^{2+} currents are found in bovine chromaffin cells: facilitation is due to the recruitment of one type. J Physiol (Lond) 432:681–707.

Bean BP (1989a) Classes of calcium channels in vertebrate cells. Annu Rev Physiol 51:367–384.

Bean BP (1989b) Neurotransmitter inhibition of neuronal calcium currents by changes in channel voltage dependence. Nature 340:153–156.

Beech DJ, Bernheim L, Hille B (1992) Pertussis toxin and voltage dependence distinguish multiple pathways modulating calcium channels of rat sympathetic neurons. Neuron 8:97–106.

Brum G, Osterrieder W, Trautwein W (1984) β-Adrenergic increase in the calcium conductance of cardiac myocytes studied with the patch clamp. Pfluegers Arch 401:111–118.

Carbone E, Swandulla D (1989) Neuronal calcium channels: kinetics, blockade and modulation. Prog Biophys Mol Biol 54:31–58.

Colquhoun D, Sigworth FJ (1983) Fitting and statistical analysis of single-channel records. In: Single-channel recordings (Neher E, Sakmann B, eds), pp 191–263. New York: Plenum.

Delcour AH, Lipscombe D, Tsien RW (1992) Shifts in gating modes are involved in the noradrenergic down-modulation of N-type Ca^{++} channels. Biophys J 61:A420.

Elmslie KS, Zhou W, Jones SW (1990) LHRH and GTP-γ-S modify calcium current activation in bullfrog sympathetic neurons. Neuron 5:75–80.

Fenwick EM, Marty A, Neher E (1982) Sodium and calcium channels in bovine chromaffin cells. J Physiol (Lond) 331:599–635.

Fox AP, Nowycky MC, Tsien RW (1987) Kinetic and pharmacological properties distinguishing three types of calcium currents in chick sensory neurones. J Physiol (Lond) 394:149–172.

Hamill OP, Marty A, Neher E, Sakmann B, Sigworth FJ (1981) Improved patch-clamp techniques for high resolution current recording from cells and cell-free membrane patches. Pfluegers Arch 391:85–100.

Hess P (1990) Calcium channels in vertebrate cells. Annu Rev Neurosci 13:337–356.

Hess P, Lansman JB, Tsien RW (1984) Different modes of Ca channel gating behaviour favoured by dihydropyridine Ca agonists and antagonists. Nature 311:538–544.

Hirning LD, Fox AP, McCleskey EW, Olivera BM, Thayer SA, Miller RJ, Tsien RW (1988) Dominant role of N-type Ca^{2+} channels in

evoked release of norepinephrine from sympathetic neurons. Science 239:57–61.
Hoshi T, Smith SJ (1987) Large depolarization induces long openings of voltage-dependent calcium channels in adrenal chromaffin cells. J Neurosci 7:571–580.
Ikeda SR (1991) Double-pulse calcium channel current facilitation in adult rat sympathetic neurones. J Physiol (Lond) 439:181–214.
Jackson MB, Wong BS, Morris CE, Lecar H, Christian CN (1983) Successive openings of the same acetylcholine receptor channel are correlated in open time. Biophys J 42:109–114.
Jones SW, Marks TN (1989a) Calcium currents in bullfrog sympathetic neurons. I. Activation kinetics and pharmacology. J Gen Physiol 94:151–167.
Jones SW, Marks TN (1989b) Calcium currents in bullfrog sympathetic neurons. II. Inactivation. J Gen Physiol 94:169–182.
Karschin A, Ho BY, Labarca C, Elroy-Stein O, Moss B, Davidson N, Lester HA (1991) Heterologously expressed serotonin 1A receptors couple to muscarinic K^+ channels in heart. Proc Natl Acad Sci USA 88:5694–5698.
Kasai H (1991) Tonic inhibition and rebound facilitation of a neuronal calcium channel by a GTP-binding protein. Proc Natl Acad Sci USA 88:8855–8859.
Kasai H (1992) Voltage- and time-dependent inhibition of neuronal calcium channels by a GTP-binding protein. J Physiol (Lond) 448: 189–200.
Kongsamut S, Lipscombe D, Tsien RW (1989) The N-type Ca channel in frog sympathetic neurons and its role in α-adrenergic modulation of transmitter release. Ann NY Acad Sci 560:312–333.
Kowalik J, Osborn MR (1968) Methods for unconstrained optimization. New York: Elsevier.
Kurachi Y, Ito H, Sugimoto T (1990) Positive cooperativity in activation of the cardiac muscarinic K^+ channel by intracellular GTP. Pfluegers Arch 416:216–218.
Lee KS (1987) Potentiation of the calcium-channel currents of internally perfused mammalian heart cells by repetitive depolarization. Proc Natl Acad Sci USA 84:3941–3945.
Lipscombe D, Madison DV, Poenie M, Reuter H, Tsien RY, Tsien RW (1988) Spatial distribution of calcium channels and cytosolic calcium transients in growth cones and cell bodies of sympathetic neurons. Proc Natl Acad Sci USA 85:2398–2402.
Lipscombe D, Kongsamut S, Tsien RW (1989) α-Adrenergic inhibition of sympathetic neurotransmitter release mediated by modulation of N-type calcium channel gating. Nature 340:639–642.
Mazzanti M, DeFelice LJ (1990) Ca channel gating during cardiac action potentials. Biophys J 58:1059–1065.
Macdonald RL, Twyman RE (1991) Biophysical properties and regulation of $GABA_A$ receptor channels. The Neurosciences 3:219–235.
McManus OB, Magleby KL (1988) Kinetic states and modes of single large-conductance calcium-activated potassium channels in cultured rat skeletal muscle. J Physiol (Lond) 402:79–120.
McManus OB, Magleby KL (1989) Kinetic time constants independent of previous single-channel activity suggest Markov gating for a large conductance Ca-activated K channel. J Gen Physiol 94:1037–1070.
Miller RJ (1992) Voltage-sensitive Ca^{2+} channels. J Biol Chem 267: 1403–1406.
Moczydlowski E, Latorre R (1983) Gating kinetics of Ca^{2+}-activated K^+ channels from rat muscle incorporated into planar lipid bilayers. Evidence for two voltage-dependent Ca^{2+} binding reactions. J Gen Physiol 82:511–542.
Moorman JR, Kirsch GE, Van Dongen AMJ, Joho RH, Brown AM (1990) Fast and slow gating of sodium channels encoded by a single mRNA. Neuron 4:243–252.
Nilius B (1988) Modal gating behavior of cardiac sodium channels in cell-free membrane patches. Biophys J 53:857–862.
Nowycky MC, Fox AP, Tsien RW (1985a) Three types of neuronal calcium channel with different calcium agonist sensitivity. Nature 316:440–443.
Nowycky MC, Fox AP, Tsien RW (1985b) Long-opening mode of gating of neuronal calcium channels and its promotion by the dihydropyridine calcium agonist Bay K 8644. Proc Natl Acad Sci USA 82:2178–2182.
Patlak JB, Ortiz M (1986) Two modes of gating during late Na^+ channel currents in frog sartorius muscle. J Gen Physiol 87:305–326.
Patlak JB, Gration KA, Usherwood PNR (1979) Single glutamate activated channels in locust muscle. Nature 478:643–645.
Penington NJ, Kelly JS, Fox AP (1991) A study of the mechanism of Ca^{2+} current inhibition produced by serotonin in rat dorsal raphe neurons. J Neurosci 11:3594–3609.
Perozo E, Bezanilla F (1990) Phosphorylation affects voltage gating of the delayed rectifier K^+ channel by electrostatic interactions. Neuron 5:685–690.
Pietrobon D, Hess P (1990) Novel mechanism of voltage-dependent gating in L-type calcium channels. Nature 346:651–655.
Plummer MR, Hess P (1991) Reversible uncoupling of inactivation in N-type calcium channels. Nature 351:657–659.
Plummer MR, Logothetis DE, Hess P (1989) Elementary properties and pharmacological sensitivities of calcium channels in mammalian peripheral neurons. Neuron 2:1453–1463.
Regan LJ, Sah DWY, Bean BP (1991) Ca^{2+} channels in rat central and peripheral neurons: high-threshold current resistant to dihydropyridine blockers and ω-conotoxin. Neuron 6:269–280.
Reuter H, Stevens CF, Tsien RW, Yellen G (1982) Properties of single calcium channels in cultured cardiac cells. Nature 297:501–504.
Rittenhouse AR, Plummer MR, Hess P (1991) Microscopic heterogeneity of N-type calcium channel gating. Soc Neurosci Abstr 17:901.
Shuba YM, Teslenko VI, Savchenko AN, Pogorelaya NH (1991) The effect of permeant ions on single calcium channel activation in mouse neuroblastoma cells: ion-channel interaction. J Physiol (Lond) 443: 25–44.
Stanley EF (1991) Single calcium channels on a cholinergic presynaptic nerve terminal. Neuron 7:585–591.
Tsien RW, Lipscombe D, Madison DV, Bley KR, Fox AP (1988) Multiple types of neuronal calcium channels and their selective modulation. Trends Neurosci 11:431–438.
Tsien RW, Ellinor PT, Horne WA (1991) Molecular diversity of voltage-dependent Ca^{2+} channels. Trends Pharmacol Sci 12:349–354.
Yue DT, Herzig S, Marban E (1990) β-Adrenergic stimulation of calcium channels occurs by potentiation of high-activity gating modes. Proc Natl Acad Sci USA 87:753–757.
Zhou J, Potts JF, Trimmer JS, Agnew WS, Sigworth FJ (1991) Multiple gating modes and the effect of modulating factors on the μI sodium channel. Neuron 7:775–785.